I S A V

Journal of Theoretical and Applied Vibration and Acoustics

journal homepage: http://tava.isav.ir

Effects of higher-order terms in aerodynamic force on the nonlinear response of a galloping PZT energy harvester

Masoud Rezaei[a], Rohollah Talebitooti[b]*

[a]*PhD Student, School of Mechanical Engineering, Iran University of Science and Technology, Narmak*
[b]*Associate Professor, School of Mechanical Engineering, Iran University of Science and Technology, Narmak*

ARTICLE INFO

Article history:
Received 18 Junuary 2020

Received in revised form
5 May 2020

Accepted 23 September 2020

Available online 5 October 2020

Keywords:
PZT energy harvesting,

Galloping oscillations,

Multiple scales method,

Nonlinear vibrations.

ABSTRACT

In this paper, the effects of higher-order terms in aerodynamic force model have been investigated on the response of galloping piezoelectric energy harvesters. The system comprised a PZT beam with a bluff body and was exposed to a fluid force. First, the dimensionless governing electromechanical equations were provided. To model the aerodynamic force, the 3rd and 7th order galloping models have been employed by adopting the quasi-steady assumption. Then, the dynamic response based on the 3rd and 7th order aerodynamic force models has been studied using a numerical integration method. Besides, an approximateanalytical solution based on the multiple scales method (MSM) has been provided. Next, the mechanical and electrical responses of the system are obtained using the MSM solutions. Finally, the optimum electrical power and the corresponding dimensionless load resistance have been obtained. The results reveal that considering higher-order terms in aerodynamic force expansion is necessary for accurate characterization of the mechanical and electrical responses.

1. Introduction

The batteries that are used as a common source of power in low-power instruments, such as wireless sensors for health monitoring in remote areas, medical implants, etc., have major drawbacks such as finite life span, costly periodical replacement, and chemical pollution. Harvesting untapped energy from the environment can be used as an alternative approach to

* Corresponding author:
E-mail address: rtalebi@ iust.ac.ir (R. Talebi)

http://dx.doi.org/10.22064/tava.2021.530769.1182

replace the batteries with sustainable, cheap, and green energy sources to achieve a local power supply and an autonomous operation. The well-known sources are kinetic energy, heat, and light energy. Among all these sources, kinetic energy is available everywhere and vast researches have been done on this area. Kinetic energy can be transmitted to electrical form using piezoelectric[1], electromagnetic [2], and electrostatic [3] mechanisms. All of these transduction mechanisms have limitations, but piezoelectric materials draw attention because they generate higher energy density and can be implemented in different sizes for different applications. Typical kinetic energy harvesting approaches are vibration and flow energy harvesting. In flow energy harvesters, the structure is placed in the flow field to catch the flow energy from flow-induced instabilities. Vibrations can occur as a result of aerodynamic instability such as vortex-induced, flutter, and galloping [4, 5] based energy harvesting. Galloping piezoelectric energy harvesters (GPEH) are composed of a PZT beam with an attached bluff body. As the fluid passes the bluff-body, the surface pressure as a result of inner circulation is produced. The pressure exerts a lift force on the bluff body. When the flow velocity increases upon a critical value, cut-in wind speed, the aerodynamic damping term dominates the intrinsic one, the structure starts to vibrate, and the amplitude of oscillation increases until the nonlinear terms limit them. This results in steady-state fixed amplitude oscillations. Consequently, electrical voltage and power are generated. Sirohi *et al*. [4] studied a GPEH with a triangular cross-section bluff body both numerically and experimentally. They showed that the air mass could affect the response of the system in reality. Sirohi *et al*.[5] investigated a GPEH with D shape cross-section bluff body, based on numerical and experimental analyses, using lumped parameter modelling and showed that the mass and the geometric properties influence the output voltage. Their experimental results approved the validity of using quasi-steady assumption in aerodynamic modelling. Abdelkefi *et al*.[6] investigated high and low Reynolds number effects on the harvested power and the cut-in-wind speed of a harvester with a square-sectioned cylinder. They reported that, unlike the high Reynolds number condition, the aerodynamic coefficients are a function of the Reynolds number in the low Reynolds number condition. Zhao *et al*.[7] studied the distributed and lumped parameter modelling of the GPEH numerically and experimentally. They showed that the lumped parameter modelling is sufficient to study the behaviour of GPEH. Abdelkefi *et al*.[8] investigated a GPEH with a square-sectioned bluff body. They reported that the maximum harvested power is accomplished via varying the load resistance. Yang *et al*.[9] showed that among all bluff bodies, the square-sectioned one produces the highest output voltage. Daqaq [10] evaluated the performance of a GPEH using actual wind statistics and power density function by adopting the lumped parameter model.

Based on the literature, the galloping aerodynamic force mainly modelled by a cubic polynomial and effects of higher-order approximations on the response of the system have not been considered. To fill this gap, this paper investigates the performance of a galloping PZT energy harvester considering third- and seventh-order polynomial representation for the aerodynamic force, both numerically and analytically. To this end, the mathematical model governing the aero-electromechanical system is provided in Sec. 2. Moreover, using the multiple scales method (MSM), the approximateanalytical solution of the problem is obtained in this section. The results are provided in Sec.3. Finally, the conclusions are given in Sec. 4.

2. Mathematical modelling

The piezoelectric energy harvester is composed of a unimorph piezoelectric cantilever beam with an attached bluff body; the system is exposed to a laminar flow. The energy harvester and its simplified electrical circuit are illustrated in Figs. 1a and b, respectively.

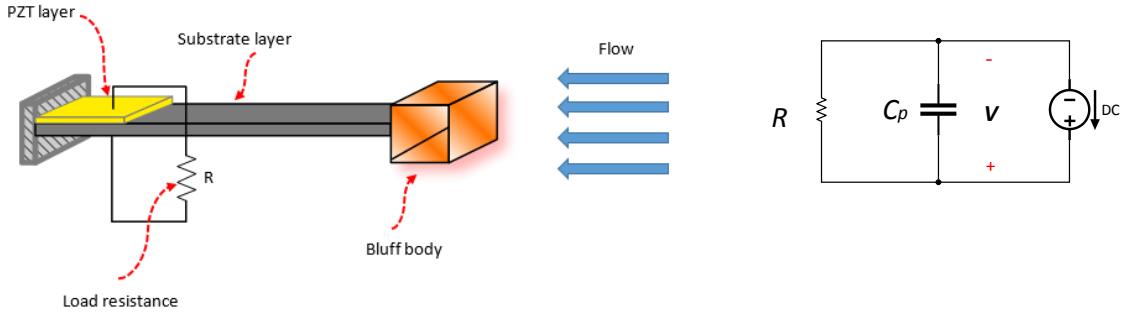

Fig. 1: (a) Schematic of the galloping PZT energy harvester (b) simplified electrical circuit

The equations governing the displacement (x) and generated voltage (V) of the piezoelectric energy harvester can be described as:

$$m\ddot{x} + c\dot{x} + kx - \theta V = F_y \tag{1}$$

$$\theta\dot{x} + C_p\dot{V} + \frac{V}{R_l} = 0 \tag{2}$$

where m, c, and k are the mass, damping, and stiffness of the coupled system, respectively. Moreover, θ, C_p, and R_l are respectively the electromechanical coupling coefficient, piezoelectric capacitance, and load resistance. Here, F_y denotes the aerodynamic force and can be represented as:

$$F_y = \frac{1}{2}\rho U^2 LD\left[a_1\frac{\dot{x}}{U} - a_3\left(\frac{\dot{x}}{U}\right)^3 + a_5\left(\frac{\dot{x}}{U}\right)^5 - a_7\left(\frac{\dot{x}}{U}\right)^7 + \cdots\right] \tag{3}$$

in which ρ, U, L, and D shows air density, flow speed, length of the bluff body, and cross-flow dimension of obstacle. In addition, a_n stands for the *n-th* aerodynamic coefficient, which is obtained empirically. Based on Ref. [11] $a_1 = 2.69$, $a_2 = 168$, $a_5 = 6270$, and $a_7 = 59900$. To generalize the results, the dimensionless forms of Eqs. (1) and (2) will be obtained by defining the following dimensionless parameters:

$$\tau = \omega_n t \;\; ; \;\; y = \frac{x}{D} \;\; ; \;\; v = \frac{C_p}{\theta D}V \;\; ; \;\; u = \frac{U}{\omega_n D} \tag{4}$$

where τ, y, and v are dimensionless time, displacement, and voltage, respectively; and ω_n is the fundamental frequency of the system.
Introducing these parameters in Eqs. (1) and (2) and truncating the force series at the fourth term yields the dimensionless equations as:

$$\ddot{y} + 2\zeta_m \dot{y} + y - \kappa v = 2\mu \bar{U}^2 \left[a_1 \frac{\dot{y}}{\bar{U}} - a_3 \left(\frac{\dot{y}}{\bar{U}} \right)^3 + a_5 \left(\frac{\dot{y}}{\bar{U}} \right)^5 - a_7 \left(\frac{\dot{y}}{\bar{U}} \right)^7 \right] \tag{5}$$

$$\dot{y} + \dot{v} + \alpha v = 0 \tag{6}$$

where the dimensionless parameters in Eqs. (5) and (6) are defined as:

$$\kappa = \frac{\theta^2}{k C_p} \quad ; \quad \mu = \frac{\rho L D^2}{4m} \quad ; \quad \alpha = \frac{1}{R_l C_p \omega_n} \tag{7}$$

The geometrical and physical data of the system are provided in Table. 1.

Table 1. The geometric and physical data [10, 12]

Parameter (symbol)	Value (unit)
Cantilever beam length	0.209 m
Effective mass (m)	0.1134 kg
Damping ratio ($\boldsymbol{\zeta_m}$)	0.003
Air density ($\boldsymbol{\rho}$)	1.25 kg/m^3
Capacitance of piezoelectric layer ($\boldsymbol{C_p}$)	187 nF
Electromechanical coupling ($\boldsymbol{\theta}$)	1.9 × 10^{-4} N/V
Bluff body length ($\boldsymbol{L}$)	0.1 m
Bluff body height ($\boldsymbol{D}$)	0.05 m

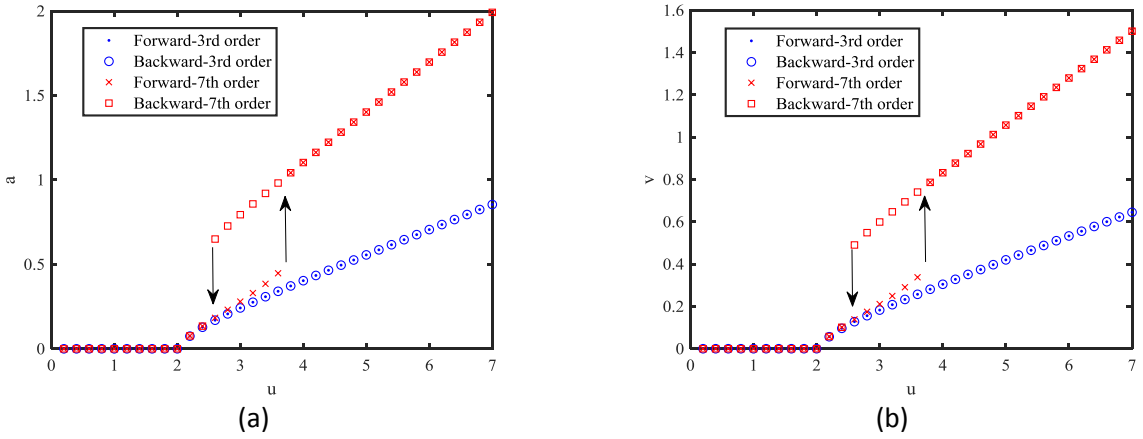

Fig.2: Variations of dimensionless (a) displacement (b) voltage versus flow speeds

It is worth to mentioning that most of the previous studies used cubic polynomial representation of the aerodynamic force by neglecting a_5 and a_7 and assessed the system response. However, here, we investigate the effects of higher-order terms and compare the system response. To this end, using the numerical integration method, the diagrams of dimensionless displacement and voltage versus dimensionless flow speed are plotted for 3rd and 7th order aerodynamic forces in Fig. 2a and 2b, respectively.

Inspecting Fig. 2, it is clear that there is a discrepancy between the results of 3rd and 7th order approximations in both displacement and voltage curves. This difference gets larger as the flow speed increases. This dictates that for the precise assessment of the dynamics of the energy harvester, especially at higher speeds, considering 7th order approximation is superior to 3rd order one. Moreover, the 7th order force responses show jump up and jump down phenomena; hence multivalued solutions exist in the responses. The jumps are denoted by arrows. In the region between two jumps, the initial conditions determine the branch to which the solution attracts. So, the results are represented considering 7th order polynomial aerodynamic force.

2.1. Approximate-Analytical Solution

In this section, the approximateanalytical solution of the problem will be obtained utilizing the multiple scales method (MSM). To this end, the following time scales are defined:

$$T_0 = t \quad ; \quad T_1 = \varepsilon t \; ; \ldots \; T_n = \varepsilon^n t \tag{8}$$

where ε is a small parameter called the bookkeeping parameter. Then, the solutions are sought in the forms of [13]:

$$y(t) = y_0(T_0, T_1) + \varepsilon y_1(T_0, T_1) + O(\varepsilon^2) \tag{9}$$

$$v(t) = v_0(T_0, T_1) + \varepsilon v_1(T_0, T_1) + O(\varepsilon^2) \tag{10}$$

(10)

The damping, electromechanical coupling, and aerodynamic force are scaled such that they appear in the first-order perturbation problem, so:

$$\zeta_m = \varepsilon\zeta_m \quad ; \quad a_1 = \varepsilon a_1 \; ; \; a_3 = \varepsilon a_3 \; ; \; a_5 = \varepsilon a_5 \; ; \; a_7 = \varepsilon a_7 \; ; \; \kappa = \varepsilon\kappa \tag{11}$$

Using chain role and defining $D_n = \partial/\partial T_n$, Eqs. (5) and (6) can be rewritten as:

$$\begin{aligned}(D_0^2 + 2\varepsilon D_0 D_1)(y_0 + \varepsilon y_1) + 2(\varepsilon\zeta_m - \mu\varepsilon a_1 u)(D_0 + \varepsilon D_1)(y_0 + \varepsilon y_1) + (y_0 + \varepsilon y_1) \\ + \frac{2\mu\varepsilon a_3}{u}\{(D_0 + \varepsilon D_1)(y_0 + \varepsilon y_1)\}^3 - \frac{2\mu\varepsilon a_5}{u^3}\{(D_0 + \varepsilon D_1)(y_0 + \varepsilon y_1)\}^5 \\ + \frac{2\mu\varepsilon a_7}{u^5}\{(D_0 + \varepsilon D_1)(y_0 + \varepsilon y_1)\}^7 - \varepsilon\kappa(v_o + \varepsilon v_1) = 0\end{aligned} \tag{12}$$

$$(D_0 + \varepsilon D_1)(v_0 + \varepsilon v_1) + \alpha(v_0 + \varepsilon v_1) + (D_0 + \varepsilon D_1)(y_0 + \varepsilon y_1) = 0 \tag{13}$$

Separating the coefficients of $\mathcal{O}(\varepsilon^0)$ and $\mathcal{O}(\varepsilon^1)$ equations yields:

$$\begin{cases} {D_0}^2 y_0 + y_0 = 0 \\ D_0 v_0 + \alpha v_0 = -D_0 y_0 \end{cases} \tag{14}$$

$$\begin{cases} {D_0}^2 y_1 + y_1 = -2D_0 D_1 y_0 - 2(\zeta_m - \mu a_1 u) D_0 y_0 + \kappa v_0 - \dfrac{2\mu a_3}{u}(D_0 y_0)^3 + \dfrac{2\mu\varepsilon a_5}{u^3}(D_0 y_0)^5 - \dfrac{2\mu\varepsilon a_5}{u^3}(D_0 y_0)^5 \\ D_0 v_1 + \alpha v_1 = -(D_0 y_1 + D_1 y_0) - D_1 v_0 \end{cases} \tag{15}$$

The solution of the zeroth-order problem (Eq. (15)) can be stated as:

$$y_0 = A(T_1)e^{iT_0} + CC \tag{16}$$

$$v_0 = \frac{i}{i+\alpha} A(T_1)e^{iT_0} + CC \tag{17}$$

where CC denotes the complex conjugate of the preceding term. Introducing the above solutions in the first equation of the first-order problem yields:

$$\begin{aligned} {D_0}^2 y_1 + y_1 = -2\{iD_1 \mathrm{A}e^{iT_0}\} - 2(\zeta_m - \mu a_1 \bar{U})\{i\mathrm{A}e^{iT_0}\} + \ \kappa \frac{i}{i+\alpha} A e^{iT_0} - \frac{2\mu a_3}{u^2}\{3iA^2\bar{A}e^{iT_o}\} \\ + \frac{2\mu a_5}{u^3}\{10A^3\bar{A}^2 i e^{iT_0}\} - \frac{2\mu a_7}{u^5}\{35A^4\bar{A}^3 i e^{iT_0}\} + NS \end{aligned} \tag{18}$$

where NS stands for non-secular terms. Assuming $A = 1/2\ a(T_1)e^{i\gamma(T_1)}$ and omitting secular terms results in:

$$-2iD_1 A - 2(\zeta_m - \mu a_1 u)Ai - \kappa \frac{1+i\alpha}{1+\alpha^2} A - \frac{6\mu a_3}{u} A^2 \bar{A} i + \frac{20\mu a_5}{u^3} A^3 \bar{A}^2 i - \frac{70\mu a_7}{u^5} A^4 \bar{A}^3 i = 0 \tag{19}$$

Separating real and imaginary parts of Eq. (19) gives the following modulation equations:

$$D_1 a = -\left(\zeta_m - \mu a_1 u - \frac{\kappa\alpha}{2(1+\alpha^2)}\right) a - \frac{3}{4}\frac{\mu a_3}{u} a^3 + \frac{5}{8}\frac{\mu a_5}{u^3} a^5 - \frac{35}{64}\frac{\mu a_7}{u^5} a^7 = 0 \tag{20}$$

$$D_1 \gamma = \frac{\kappa}{2(1+\alpha^2)} \tag{21}$$

Setting $D_1 a = 0$, the following equation governing the amplitude of the steady-state response (a) is obtained:

$$-\left(\zeta_m - \mu a_1 u - \frac{\kappa\alpha}{2(1+\alpha^2)}\right) a - \frac{3}{4}\frac{\mu a_3}{u} a^3 + \frac{5}{8}\frac{\mu a_5}{u^3} a^5 - \frac{35}{64}\frac{\mu a_7}{u^5} a^7 = 0 \tag{22}$$

Moreover, based on Eq. (17), the steady-state voltage amplitude can be stated as:

$$\mathrm{v} = \frac{1}{\sqrt{(1+\alpha^2)}} a \tag{23}$$

3. Results and Discussions

In this section, the response of the galloping PZT energy harvester will be represented. First, the onset of instability speed will be obtained. Due to the fact that at the instability threshold the nonlinear terms are negligible compared to linear ones, a linear analysis will be carried out to obtain the onset of instability. The aero-electromechanical equation has three eigenvalues and galloping instability occurs as the real part of any of the eigenvalues turns from negative to positive. Hence, to obtain the onset of instability speed, the real part of eigenvalues should be plotted versus flow velocity. This is illustrated in Fig. 3 for three different damping values.

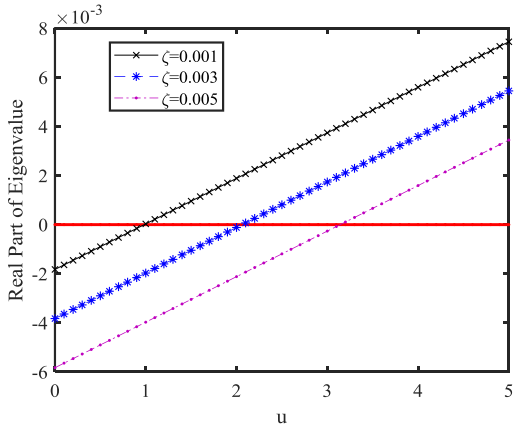

Fig. 3: Onset of instability speed for three different damping values

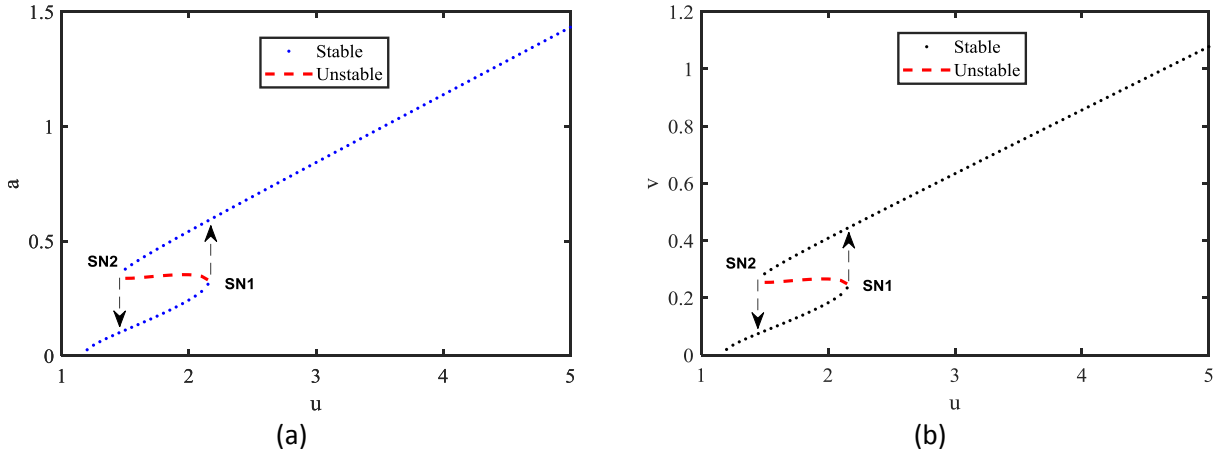

Fig. 4: (a) deflection (b) voltage versus flow speed. Dots and dashed lines represent the stable and unstable solutions, respectively

As it is clear from Fig. 3, increasing the damping value increases the onset of instability speed. By using MSM solution, the displacement and voltage of the system versus flow speed are plotted in Fig. 4a and b, respectively. As illustrated in Fig. 4a, the deflection of the beam increases by increasing the flow speed. Moreover, the voltage amplitude is amplified by adding the flow velocity. This is in agreement with Eq. (23). Besides, as obtained from the numerical

solution in Fig. 2, the multivalued solutions between jump points are also shown in Figs. 4a and b. In addition to the numerically obtained graphs, the unstable branches of the deflection and voltage responses can be observed in the graphs obtained by MSM. Besides, in the forward sweep path, the mechanical and electrical responses undergo a saddle-node bifurcation at SN1 point. At this point, the deflection and voltage both jump up from the lower branch to the higher one. On the other hand, in the backward sweep, the responses experience a saddle-node bifurcation at SN2 and they jump down to the lower branches. It is worth mentioning that the response in the multivalued sections depends on the initial conditions. To assess the effects of time constant ratio, the diagrams of displacement and power versus dimensionless time constant ratio (α) are plotted in Fig. 5.

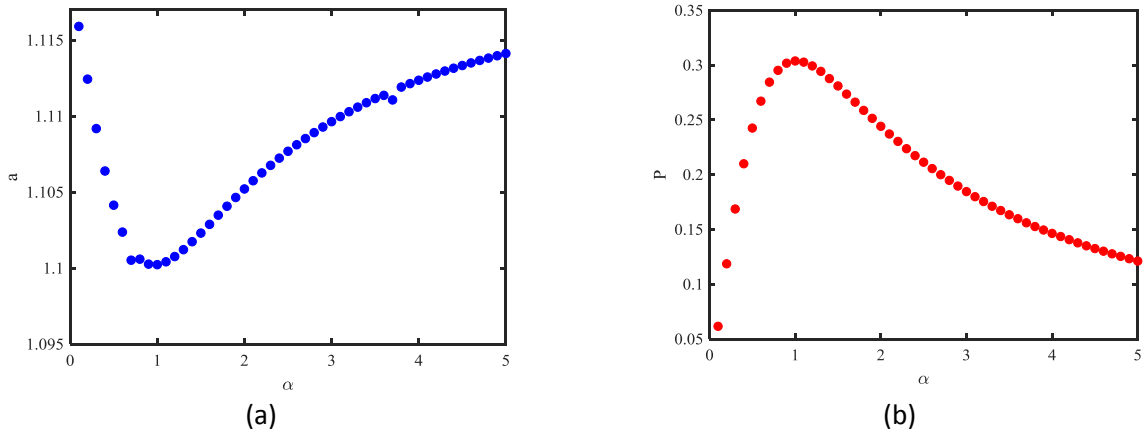

Fig. 5: (a) displacement (b) power versus dimensionless time constant ratio

Based on Fig. 5a, at the special value of α, the deflection reaches to its minimum value. This is due to the fact that, at this value of α, the coupled damping is maximum. On the other hand, in the region of minimum displacement, the output power has its maximum. Specifically, at this portion of α, the energy transfer is maximized. The maximum power is called optimum power and the corresponding value of α is referred to as optimum time constant ratio.

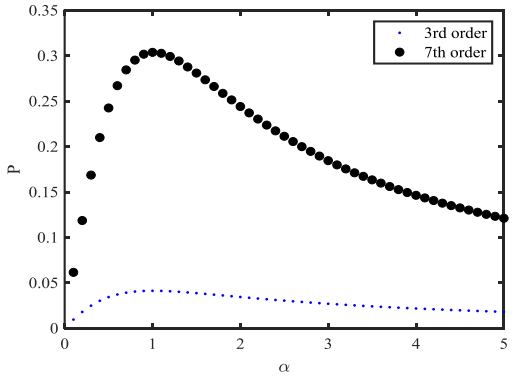

Fig. 6: Power versus time constant ratio for 3rd and 7th order approximation

Finally, the effect of aerodynamic force modelling can be assessed by comparing optimum powers. To this end, the graphs of power against α for the scenarios of 3rd and 7th order aerodynamic force are given in Fig. 6. As it is obvious from Fig. 6, there is a significant difference between 3rd and 7th order force in estimating the output power. In other words, the 3rd order model underestimates the output power. Hence, to acquire a correct estimation, considering the higher orders is necessary.

4. Conclusion

In this paper, the influences of aerodynamic force representation on the dynamical response of a galloping PZT energy harvester were studied. The was system composed of a cantilever PZT beam with an attached bluff body. First, the electromechanical equations were provided. Then, the system response was investigated for 3rd and 7th order approximations using a numerical integration method. Results disclosed that the higher-order terms play a significant role in the system response. Then, an approximateanalytical solution utilizing the multiple scales method was obtained. Also, by using this solution, the stable and unstable branches of response were obtained and the bifurcation points and jump regions were determined. It was revealed that, on the contrary to the 3rd order model, when the 7th order model is used, the responses exhibit saddle-node bifurcations. Finally, comparing the optimum power of the system based on the different approximations demonstrated that considering the higher-order terms is necessary for the accurate assessment of the system response.

References

[1] M. Rezaei, R. Talebitooti, S. Rahmanian, Efficient energy harvesting from nonlinear vibrations of PZT beam under simultaneous resonances, Energy, (2019).
[2] S.P. Beeby, R. Torah, M. Tudor, P. Glynne-Jones, T. O'donnell, C. Saha, S. Roy, A micro electromagnetic generator for vibration energy harvesting, Journal of Micromechanics and microengineering, 17 (2007) 1257.
[3] S. Boisseau, G. Despesse, B.A. Seddik, Electrostatic conversion for vibration energy harvesting, arXiv preprint arXiv:1210.5191, (2012).
[4] J. Sirohi, R. Mahadik, Piezoelectric wind energy harvester for low-power sensors, Journal of Intelligent Material Systems and Structures, (2011) 1045389X11428366.
[5] J. Sirohi, R. Mahadik, Harvesting wind energy using a galloping piezoelectric beam, Journal of vibration and acoustics, 134 (2012) 011009.
[6] A. Abdelkefi, M.R. Hajj, A.H. Nayfeh, Power harvesting from transverse galloping of square cylinder, Nonlinear Dynamics, 70 (2012) 1355-1363.
[7] L. Zhao, L. Tang, Y. Yang, Comparison of modeling methods and parametric study for a piezoelectric wind energy harvester, Smart materials and Structures, 22 (2013) 125003.
[8] A. Abdelkefi, Z. Yan, M.R. Hajj, Modeling and nonlinear analysis of piezoelectric energy harvesting from transverse galloping, Smart materials and Structures, 22 (2013) 025016.
[9] Y. Yang, L. Zhao, L. Tang, Comparative study of tip cross-sections for efficient galloping energy harvesting, Applied Physics Letters, 102 (2013) 064105.
[10] M.F. Daqaq, Characterizing the response of galloping energy harvesters using actual wind statistics, Journal of Sound and Vibration, 357 (2015) 365-376.
[11] G.R. Cook, E. Simiu, Chaotic motions of forced and coupled galloping oscillators, Journal of Wind Engineering and Industrial Aerodynamics, 36 (1990) 1083-1094.

[12] M. Rezaei, R. Talebitooti, Investigating the Effects of Aerodynamic Force Model on the Response of a Galloping PZT Energy Harvester, in: کنفرانس دو سالانه بین المللی مکانیک جامدات تجربی, undefined, 1398.
[13] A.H. Nayfeh, Perturbation methods, John Wiley & Sons, 2008.